Communication in Physical Sciences, 2023, 9(4): 412-437

Protonation-Induced Structural and Spectroscopic Variations in Molecular Species: A Computational Study on N_2, H_2, CO, CS, and PH_3

John Paul Shinggu*, Emmanuel E. Etim and Alfred I. Onen
Received: 23 April 2023/Accepted 02 August 2023/Published 04 August 2023

Abstract: *This research presents computational studies on the influence of protonation on the structural and spectroscopic properties of molecules, with a focus on N_2, CO, H_2, CS, and PH_3. Computational calculations were performed using various methods and levels of theories, including G4, MP2/6-311*, MP2/CC-pvdz, CCSD/CC-pvdz, and W2U. Calculations of thethe proton affinity (PA) and the examination of the effects of protonation on the bond lengths, bond angles, vibrational frequencies, dipole moment, and rotational constants of various molecules were also performed. The results of the calculation displayed a significant variation in molecular geometries, vibrational frequencies, dipole moments, and proton affinity protonation. Protonation was observed to be a precursor to the e formation of charged species and therefore highlighted, their potential as reactive intermediates in chemical reactions. The computational methods employed in this study clearly show that adopted methods can effectively be employed to describe the protonation-induced structural and spectroscopic variations in the molecules. These findings contribute to a better understanding of protonation processes in diatomic molecules and have implications for various fields, including chemistry, spectroscopy, and theoretical studies.*

Keywords: Proton affinity, Spectroscopic properties, Computational methods, Bond lengths, Bond angles

John P. Shinggu*
Department of Chemical Sciences, Federal University Wukari
Email: johnshinggu@gmail.com

Emmanuel E. Etim
Department of Chemical Sciences, Federal University Wukari
Email: emmaetim@gmail.com
Orcid id: 0000-0001-8304-9771

Alfred I. Onen
Department of Chemical Sciences, Federal University Wukari
Email: alfredonen@gmail.com

1.0 Introduction

Computational methods have revolutionized the field of chemistry because it is useful in the prediction and of molecular, electronic, physiochemical, topological, molecular and other properties of molecules to a very good degree depending on the level of theory the calculation is performed and the availability of parameterization concerning the compound of interest (Eddy and Ita, 2011a-b). Although computational methods have shown significant reliability in several research fields, one area of particular interest is the employment of computational methods to study protonated molecular species because of the significance of the results expected in astrophysics and astrochemistry (Keith *et al*., 2021). Theoretical-computational studies have shown that under extreme conditions in the interstellar medium (ISM), complexes of noble gases may be formed. These observations have generated a wide range of possibilities, and the study of

these protonated molecular species is essential to better understand the chemical bonding and electron sharing in these systems (Montes and Prosmiti, 2021; Chen *et al*., 2020).

The addition of a proton (H^+) to a molecule, has also been found to be significant in the understanding of some critical roles of protonated species in various chemical and biological processes (Nair and Pathak, 2021; Etim *et al*., 2020). The application of some methods such as Gaussian has been reported to be effective in opening knowledge on the structural, energetic, and spectroscopic aspects of protonated species. (Krynski and Rossi, 2021).

Cations represent about 10% of all known interstellar and circumstellar molecular species. Almost 80% of these cations are protonated species with known interstellar medium (ISM) neutral equivalents (Etim and Arunan, 2015). Because H_3^+ is abundant in molecular clouds, any neutral molecular species in ISM may be protonated using a gas phase method. In the gas phase, protonated species are generated predominantly by interacting with neutral species with abundant interstellar ions such as H^+, C^+, He^+, HCO^+ and H_3O^+ (Caselli *et al*., 2019). Natural antecedents of neutral species include protonated species (Defrees and McLean, 1986). Thus, whether astronomically detected or yet to be discovered, a protonated species and its neutral equivalent have a direct link. Hence, because of the absence of a permanent dipole moment, protonated interstellar species are significant not only for simulating interstellar cloud chemistry but also for signalling the presence and abundance of non-polar neutral species, which are difficult to detect through rotational transitions (Etim *et al*., 2017). For example, N_2H^+ and $HOCO^+$ were discovered decades before their neutral equivalents, N_2 and CO_2, respectively. These protonated species' observations corroborate the presence and detectability of the neutral counterparts, which leads to more searches for these neutral species, which eventually leads to successful astronomical observations (Turner, 2020; Knauth *et al*., 2004; Thaddeus *et al*., 1981). Two of the five successful interstellar molecular species discovered in 2015 are cations, while one is a protonated species ($NCCNH^+$). The discovery of $NCCNH^+$, whose non-polar neutral equivalent, NCCN, is yet unknown, emphasizes the significance of protonated molecular species (Agundez, 2015; Cabezas *et al*., 2022).

The energetic properties of protonated species have been extensively studied computationally. Researchers have employed various computational methods, including DFT and ab initio calculations, to determine protonation energies, reaction energies, and binding energies (Noble *et al*., 2019). Cramer *et al*., (2013) utilized computational chemistry to investigate protonation and redox reactions, providing insights into the energetics and thermodynamics of protonated species (Cramer *et al*., 2013). These energetic analyses contribute to understanding the stability and reactivity of protonated molecular species.

Computational studies have revealed the impact of protonation on the structural properties of molecules. By employing ab initio calculations and molecular dynamics simulations, researchers have investigated the conformational changes induced by protonation (Ben-Shimon *et al*., 2013). For instance, Nguyen *et al.* (2014) explored the conformational dynamics of protonated biomolecules in the gas phase, highlighting the influence of protonation on molecular flexibility and shape (Nguyen *et al*., 2014). These studies provide valuable insights into the effects of protonation on molecular structure and geometry (Re *et al*., 2018). By calculating vibrational frequencies, electronic transitions, and NMR chemical shifts, researchers have gained insights into the effects of protonation on spectroscopic signatures (Benkyi *et al*., 2019). Wang *et al*., (2020) reviewed the electronic structure calculations of protonated

organic molecules, emphasizing the importance of computational methods in predicting and interpreting experimental spectra (Wang *et al*., 2020). These spectroscopic characterizations aid in the identification and understanding of protonated molecular species.

Protonated molecules are formed because of the conditions in ISM, by a dissociative recombination process, in which a positive molecular ion interacts with an electron to produce neutral species. It remains one of the primary production pathways for interstellar molecular species (Herbst, 2017; Larsson and Orel, 2008; Noble *et al*., 2019). The most stable protonated species should be more numerous (assuming reaction routes do not differ much) and hence simpler to detect than its less stable cousin (Etim *et al*., 2017). This is due to the lower proton affinity species' ability to swiftly transfer its proton and return to its neutral state, in contrast to its isomer, which has a higher proton affinity value for the identical neutral species and prefers to remain protonated. The low proton affinity of the protonated species suggests strong reactivity, which diminishes interstellar abundance and complicates astronomical discovery (Etim and Oko, 2020).

In this research, we provided a comprehensive study of the vibrational frequencies and molecular properties of protonated molecular species using computational methods. We explored the bond lengths, bond angles, vibrational frequencies, rotational constants, dipole moments, and binding energy of these species, providing insights into their chemical and physical properties (Baiz *et al*., 2020).

2.0 Computational Methods

The GAUSSIAN 09 suite of programs was used to execute all of the quantum chemical calculations in this research (Frisch *et al*., 2009). Few neutral species investigated in this study have experimentally determined Proton affinities while their protonated analogs were calculated computationally. Computational techniques that can compute Proton affinities with high accuracy for neutral species having experimentally known Proton affinities and may be able to predict accurate proton affinity values for species that do not have empirically documented Proton affinities. Several high-level ab initio procedures were utilized to generate extremely accurate Proton affinities for all of the systems discussed here. Other parameters such as the bond length, bond angles, vibrational frequencies, dipole moments and rotational constants were also calculated. The Møller-Plesset second-order perturbation theory method (MP2) was used with the 6-311* basis set and the correlation-consistent Polarized Valence Double Zeta (CC-Pvdz) basis set (Mata, 2010). In addition to the methods described above, the coupled cluster method was also used with the correlation-consistent Polarized Valence Double Zeta (CC-Pvdz) basis set (Bodenstein and Kvaal, 2020). Compound models such as; the Gaussian theory (G4) and the Weizmann theory (W2U), were used to forecast correct Proton affinities for all of the systems under study (Chester, 2019; Frisch *et al*., 2009). These compound models provided good precision at a low computational cost. They are made up of various component computations, the results of which are subsequently integrated in a predisposed manner.

3.0 Results and Discussion

The protonated molecular species are unique in computational chemistry because of the irregularity or rather the absence of definite enthalpy of formation. A proton can attach to a neutral molecule in more than one place, resulting in distinct protonated species and proton affinities (proton affinities) corresponding to the same neutral species. The magnitude of the proton affinity indicates the intensity of the protonated species' stability. A greater proton affinity value simply means that the proton is tightly bound to the neutral

molecule, implying that the protonated species is more stable. In this situation, we discovered that greater proton affinity-associated compounds were observed than their abundant counterparts. Of course, there is a direct relationship between molecular species stability and interstellar abundance, which affects astronomical measurements.

3.1 Nitrogen Gas N_2

3.1.1 Proton Affinity

The proton affinity of N_2 (nitrogen gas) can be estimated based on the proton affinity of nitrogen, which is approximately 118 kcal/mol. Since N_2 is a diatomic molecule composed of two nitrogen atoms, adding a proton to N_2 would lead to the formation of N_2H^+ cation. The proton affinity of N_2 reflects the tendency of the molecule to accept a proton and form the N_2H^+ species, and it provides valuable information about the reactivity and chemical behavior of nitrogen gas in various chemical processes and reactions. Since the proton affinity of N_2H is relatively low it can be said to be less stable. Table 1a shows the proton affinity values for N_2. The results show that the CCSD method provides the most accurate result and hence can be used to predict the proton affinity values for other molecules.

3.1.2 Bond lengths and Bond angles

The protonation of N_2 to form N_2H^+ directly influenced a change the bond length. The bond lengths of N_2H^+ can be seen in Table 1b.

Table 1a. Proton Affinity values for N_2

Method		Proton Affinity (KCal/mol)	Error
	Experimental	118.00	-
	G4	118.37	0.37
N_2H	**MP2/CC-pvdz**	118.11	0.11
	CCSD/ CC-pvdz	117.97	0.03
	W2U	116.60	1.4
	MP2/6-311*	118.20	0.20

Fig. 1a. Optimized geometry of N_2 and its protonated analog

Table 1b. Bond length and Bond angle values of N_2H^+ and N_2

Method	Bond Lengths (Å) N_2H^+		Bond Angle (°)	Bond Lengths (Å) N_2
	R(N1-N2)	**R(N2-H3)**	**A(N1-N2-H3)**	**N1- N2**
Experimental	-	-	180	1.090
G4	1.092	1.037	180°	1.099
MP2/cc-pvdz	1.112	1.048	180°	1.145
CCSD/ cc-pvdz	1.136	1.080	180°	1.090
W2U	1.085	1.036	180°	1.090
MP2/6-311*	1.123	1.044	180°	1.120

3.1.3 Rotational Constants

The rotational constants of molecules depend on their molecular structures and masses. In the case of N_2 (nitrogen gas), it is a homonuclear diatomic molecule with two nitrogen atoms of the same mass, resulting in two identical rotational constants, B and C. Due to the symmetric and linear nature of N_2, it has a rotational constant A of 0.00 as there is no rotational energy associated with rotation around the molecular axis, while B and C are 49.088 and 49.088 Ghz respectively. On the other hand, N_2H^+ (Diazenylium) is a heteronuclear diatomic molecule, consisting of nitrogen and hydrogen atoms. The presence of two different elements with different masses leads to non-identical rotational constants. N_2H^+ has a rotational constant A of 0.00, similar to N_2, while its rotational constants B and C are within the range of 43.8 and 47.3 GHz due to the asymmetry introduced by the hydrogen atoms, which affects its rotational behavior. The results can be seen in Table 1c.

Table 1c. Rotational constant values for N_2 and N_2H^+

	Method	Rotational Constants (Ghz)		
		A	B	C
N_2	**Experimental**	0.000	49.088	49.088
	G4	0.000	49.531	49.531
	MP2/cc-pvdz	0.000	47.681	47.681
	CCSD/ cc-pvdz	0.000	48.268	48.268
	W2U	0.000	60.600	60.600
	MP2/6-311*	0.000	48.288	48.288
N_2H^+	**Experimental**	-	-	-
	G4	0.000	46.819	46.819
	MP2/cc-pvdz	0.000	43.813	43.813
	CCSD/ cc-pvdz	0.000	45.312	45.312
	W2U	0.000	47.348	47.348
	MP2/6-311*	0.000	43.814	43.814

3.1.4 Dipole Moment

N_2 (nitrogen gas) has no dipole moment because it is a homonuclear diatomic molecule composed of two nitrogen atoms bonded together, sharing electrons equally. Since nitrogen has the same electronegativity, the bond is nonpolar, resulting in an even distribution of electron density, and no permanent charge separation. Conversely, N_2^+ H (Diazenylium) has a calculated dipole moment ranging from 3.12 - 3.16 Debye because it is a heteronuclear triatomic molecule with nitrogen and hydrogen atoms. Nitrogen's higher electronegativity than hydrogen leads to a polar covalent bond, creating an uneven distribution of electron density. The asymmetric arrangement of hydrogen atoms relative to nitrogen causes a permanent dipole, with the positive end closer to hydrogen and the negative end closer to nitrogen, resulting in the observed dipole moment.

3.1.5 Vibrational Frequencies

Due to its linear, symmetric structure, N_2 (nitrogen gas) has only one frequency in its rotational spectrum. N_2 is a homonuclear diatomic molecule composed of two nitrogen atoms bound together, and its rotational motion is characterized by a single moment of inertia. As a result, the rotating energy levels of N_2 produce a single set of equally spaced spectral lines, giving birth to a single frequency. Because it is a heteronuclear diatomic molecule

consisting of nitrogen and hydrogen atoms, N_2H^+ (hydrazine) exhibits four frequencies in its rotational spectrum. Because of their asymmetric configuration, these atoms have distinct moments of inertia for their three primary axes of rotation. N_2H^+ therefore has four separate sets of rotating energy levels and spectral lines giving rise to four frequencies in its rotational spectrum.

Table 1d. Dipole moment values for N_2H^+ and N_2

	Method	Dipole Moment (Debye) N_2H^+	Dipole moment (Debye) N_2
	Experimental	-	0.00
	G4	3.120	0.00
N_2H^+	**MP2/cc-pvdz**	3.161	0.00
	CCSD/ cc-pvdz	3.145	0.00
	W2U	3.120	0.00
	MP2/6-311*	3.148	0.00

Table 1e. Vibrational frequencies of N_2H

		Vibrational Frequencies (cm^{-1})				
Experimental		**G4**	**CCSD/ PVDZ**	**W2U**	**MP2/6-311***	**MP2/CC-PVDZ**
-		729.9889	716.2456	135.2313	741.5781	711.5212
N_2H^+	-	729.9889	716.2456	135.2313	741.5781	711.5212
-		2369.959	2259.412	4.067500	2410.112	2130.417
-		3419.213	3396.115	664.4350	3411.378	3387.868
N_2	1733	2430.950	2019.256	2460.401	2138.761	2176.2517

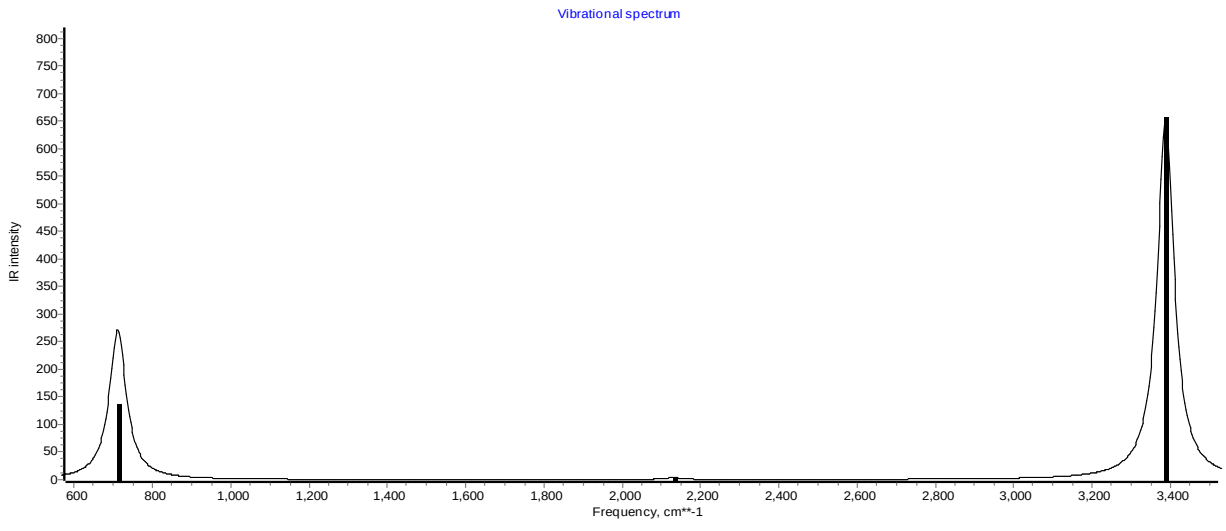

Fig. 1b. Calculated IR Intensities for N_2H^+

3.2 Carbon Monoxide CO

3.2.1 Proton Affinity Values for CO

The proton affinity of carbon monoxide (CO), which corresponds to the formation of the formyl cation (HCO^+), is approximately 142.0 kcal/mol. This value indicates the energy released when a proton is added to CO, forming the HCO^+ ion. The relatively high proton affinity reflects the strong attraction between the CO molecule and the proton, facilitated by the electronegative oxygen atom, which stabilizes the positive charge of HCO^+ through resonance. On the other hand, the second proton affinity of carbon monoxide, approximately 101.9 kcal/mol, corresponds to the energy released when another proton is added to the formyl cation (HCO^+), leading to the formation of protonated carbon monoxide (HOC^+). The lower proton affinity for the second protonation can be attributed to the increased positive charge density on the already protonated oxygen atom, reducing the ease of adding a second proton. Thus, the difference in proton affinity values underscores the differing stability and reactivity of the formyl cation (HCO^+) and protonated carbon monoxide (HOC^+).

Table 2a. Proton affinity values of CO

Method	Proton attached to O atom		Proton attached to C atom	
	PA (kcal/mol)	Error	PA (kcal/mol)	Error
Experimental	101.90	NA	142.00	NA
MP2/6-311^{++}G**	97.63	4.27	144.61	-2.60
MP2/cc-pVDZ	99.00	2.9	144.68	-2.68
CCSD// cc-pVDZ	104.95	-3.05	144.36	-2.36
G4	107.97	-6.07	142.93	-0.93
W2U	102.84	-0.94	140.12	1.88

3.2.2 Bond lengths and bond angle of HCO

With regards to the bond length of Carbon monoxide, the G4 method provided the most accurate results with regard to the experimental data, hence the bond lengths of HCO^+ and CHO^+ can be interchanged with the results obtained from the G4 method. The results can be seen in Table 2b.

Fig. 2a. Optimized geometries of CO, HCO^+ and HOC^+

Table 2b. Bond lengths and bond angles of CO, HCO^+ and HOC^+

Bond lengths, R (Å) and bond angles, A(º) of CO, HCO^+ and HOC^+							
		Expt	G4	CCSD/ CC-PVDZ	W2U	MP2/6-311*	MP2/CC-PVDZ
	R(H1-O2)	-	1.092	0.999	0.995	1.019	1.004
HOC^+	R(C2-O3)	-	1.037	1.167	1.153	1.044	1.169
	A(H1-O2-C3)	-	180º	180º	180º	180º	180º
HCO^+	R(H1-C2)	-	1.097	1.106	1.095	1.105	1.103
	R(C2-O3)	-	1.107	1.115	1.100	1.121	1.127
	A(H1-C2-O3)	-	180º	180º	180º	180º	180º
CO	R(C1-O2)	1.130	1.131	1.138	1.124	1.128	1.147

3.2.3 Rotational Constants

Both molecules consist of the same atoms (hydrogen, carbon, and oxygen) but have different molecular geometries, resulting in different rotational constants. The protonation of carbon monoxide reduced the rotational constants of the two species from 50.665 Ghz to 44.706 Ghz due to geometrical changes.

For HCO^+ (formyl radical), the rotational constant is approximately 44.706 GHz. The geometry of HCO^+ is linear, meaning the hydrogen, carbon, and oxygen atoms are arranged in a straight line. The linear geometry leads to a specific moment of inertia, resulting in a particular rotational constant. On the other hand, for HOC^+ (carbonyl cation), the rotational constant is also approximately 44.706 GHz.

Table 2d. Rotational constant values for CO, $HOC^+$and HCO^+

Method		Rotational Constants (Ghz)		
		A	**B**	**C**
	Experimental	0.000	50.665	50.665
	G4	0.000	57.634	57.634
CO	**MP2/cc-pvdz**	0.000	57.634	57.634
	CCSD/ cc-pvdz	0.000	56.974	56.974
	W2U	0.000	57.634	57.634
	MP2/6-311*	0.000	57.634	57.634
Experimental		-	-	-
	G4	0.000	44.511	44.511
HOC^+	**MP2/cc-pvdz**	0.000	44.511	44.511
	CCSD/ cc-pvdz	0.000	44.511	44.511
	W2U	0.000	44.511	44.511
	MP2/6-311*	0.000	44.511	44.511
	Experimental	-	-	-
	G4	0.000	44.706	44.706
HCO^+	**MP2/cc-pvdz**	0.000	44.706	44.706
	CCSD/ cc-pvdz	0.000	44.040	44.040
	W2U	0.000	47.348	47.348
	MP2/6-311*	0.000	44.706	44.706

Unlike HCO^+, HOC^+ has a non-linear geometry, with the carbon atom forming a double bond with oxygen and a single bond with hydrogen. Despite the different arrangement of atoms, the masses involved and the overall molecular structure still lead to a rotational constant value close to that of HCO.

In summary, even though HCO^+ and HOC^+ have different molecular geometries, their rotational constants are the same, approximately 44.706 GHz, due to the specific masses and structural arrangements of their constituent atoms.

3.2.4 Dipole Moment values of HOC^+ and HCO^+

CO has a dipole moment of 0.122 Debye. The dipole moment in CO is much smaller compared to HOC^+ and HCO^+ because it is a linear molecule with a polar C=O bond. Although the C=O bond is polar due to the electronegativity difference between carbon and oxygen, the linear geometry causes the partial positive and negative charges to cancel

each other out to some extent, resulting in a smaller overall dipole moment.

The dipole moment of HCO^+ arises primarily from the polar C=O bond. Oxygen is more electronegative than carbon, leading to an unequal sharing of electrons. The oxygen end of the C=O bond is negatively charged, while the hydrogen and carbon ends have partial positive charges. The molecule's geometry also influences the dipole moment, but it is relatively smaller compared to HOC^+ due to the asymmetry introduced by the presence of only one hydrogen atom.

The dipole moments of HOC^+, HCO^+, and CO differ due to the presence of polar bonds and their respective molecular geometries. CHO^+ has the largest dipole moment due to multiple polar bonds and its molecular structure, while HCO^+ has a lower dipole moment compared to HOC^+ due to its asymmetric structure with fewer polar bonds. CO, being linear, has the smallest dipole moment among the three due to partial charge cancellation caused by its linear geometry. From the results in Table 2e, the dipole moment of carbon monoxide was accurately predicted by the G4 method.

Table 2e. Dipole Moment values for HOC^+ and HCO^+ and CO

Method	Dipole Moment (Debye) HOC^+	Dipole Moment (Debye) HCO^+	Dipole Moment (Debye) CO
Experimental	-	-	0.1220
G4	2.5703	3.7086	0.1414
MP2/cc-pvdz	2.5680	4.2452	0.2468
CCSD/ cc-pvdz	2.3366	4.3088	0.2788
W2U	2.3366	3.7346	0.0812
MP2/6-311*	2.4561	4.1254	0.2423

3.2.5 Vibrational Frequencies CO, HCO^+ and HOC^+

CHO^+ and HCO^+ have four vibrational frequencies and three sharp peaks in their infrared spectra due to the presence of four vibrational modes in their asymmetric linear structures. Asymmetric linear molecules have three vibrational degrees of freedom: two bending modes and one stretching mode. Additionally, they have a fourth vibrational mode associated with their asymmetric internal rotation. Each vibrational mode corresponds to a specific vibrational frequency, and the different combinations of these modes give rise to the four observed vibrational frequencies in the spectra. In contrast, CO is a linear molecule with a symmetric structure, possessing only two vibrational degrees of freedom: one stretching mode and one bending mode. As a result, it exhibits only one peak in the infrared spectrum, corresponding to its single vibrational frequency.

Table 2f. Vibrational Frequencies of CO, HOC^+ and HCO^+

		Vibrational Frequencies (cm^{-1})				
	Experimental	**G4**	**CCSD/ CC-PVDZ**	**W2U**	**MP2/6-311***	**MP2/CC-PVDZ**
	-	868.3371	832.4	864.2282	841.3145	821.7077
HOC^+	-	868.3371	832.4	864.2282	841.3145	821.7078
	-	2257.7114	2251.3	2276.7216	2265.1891	2128.2312
	-	3225.5500	3267.9	3217.6277	3203.8473	3277.5588

CO	2143.0000	2204.7031	2209.9952	2230.1741	2241.3098	2116.738
	-	242.4763	182.4	157.9842	235.1352	278.5
HCO^+	-	242.4763	182.4	157.9842	235.1352	278.5
	-	1971.8748	1973.6	1976.6494	1996.8912	1944.0
	-	3440.2856	3465.1	3419.0171	3211.3834	3399.8

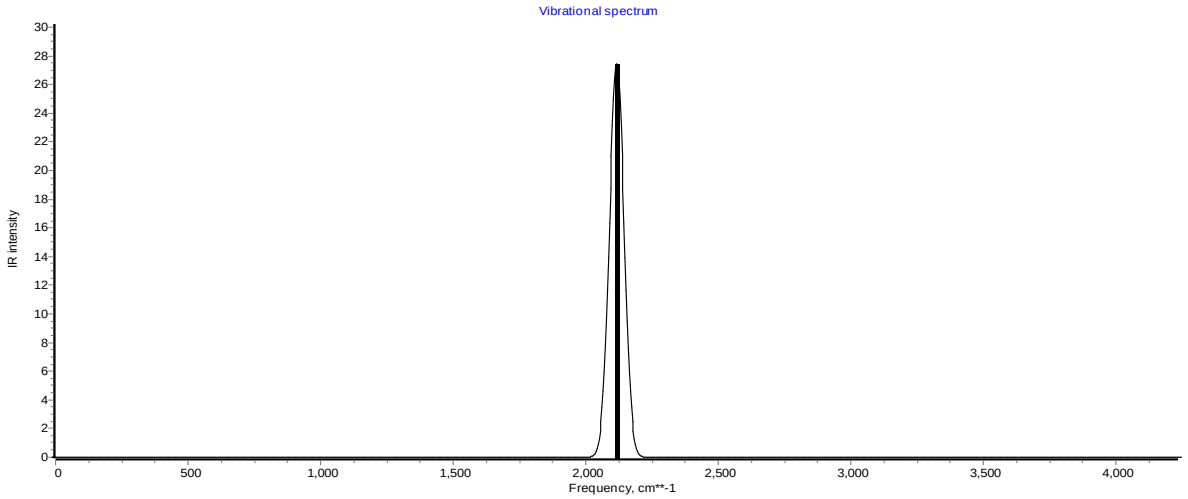

Fig. 2b. Calculated IR Intensities for CO

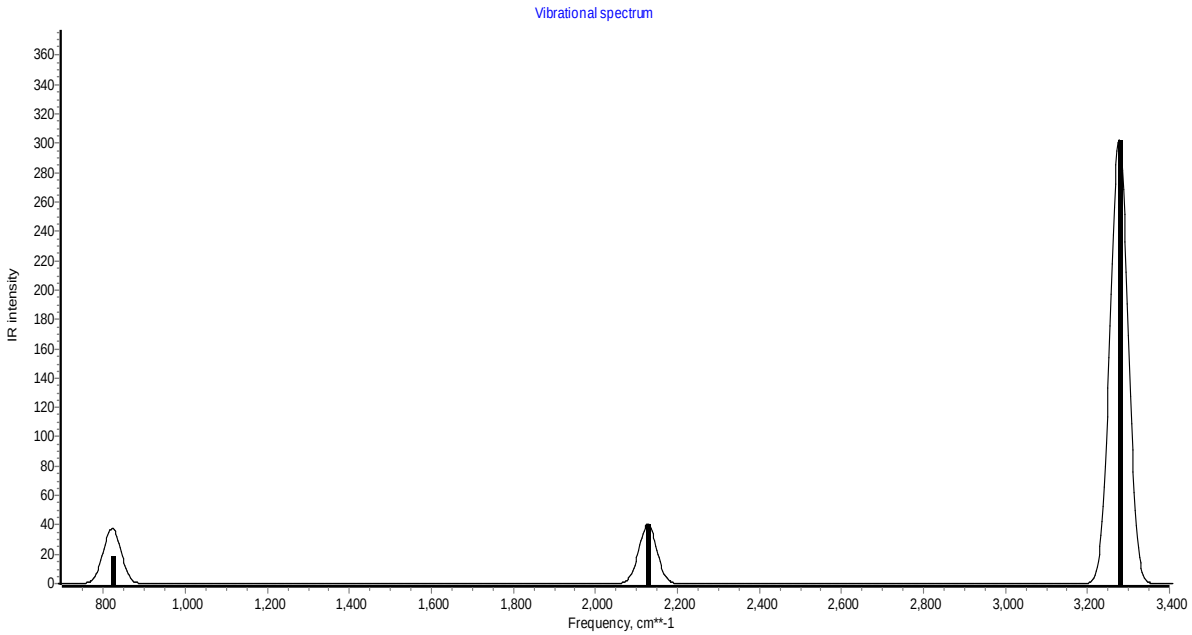

Fig. 2c. Calculated IR Intensities for HCO^+

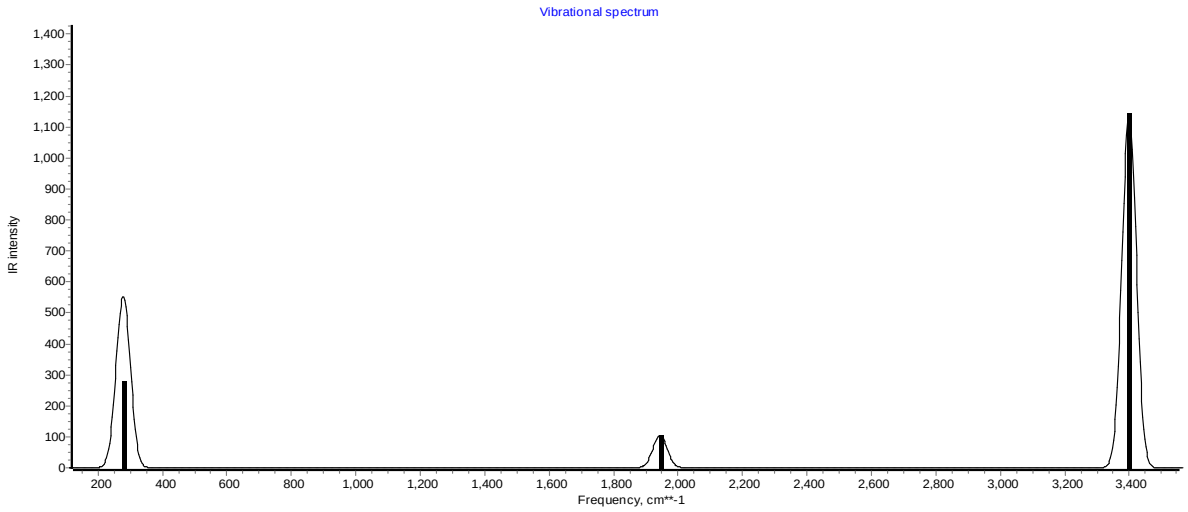

Fig. 2d. Calculated IR Intensities for HOC^+

3.3 Carbon Monosulfide CS

3.3.1 Proton Affinity

Carbon monosulfide (CS) has a proton affinity of 189.2 kcal/mol, which is the energy necessary to add a proton (H^+) to a CS molecule, resulting in the positively charged cation HCS^+. The transfer of a proton to the carbon atom in carbon monosulfide results in the production of the HCS^+ cation. Carbon monosulfide has a relatively high proton affinity, indicating a favourable inclination to take a proton and form the HCS^+ species. This feature is important in a variety of chemical processes, especially in acidic conditions where protonation reactions are common. Understanding carbon monosulfide's proton affinity gives useful insights into its chemical behavior, reactivity, and participation in proton-transfer reactions, making it relevant in both theoretical and practical parts of chemistry.

The CCSD method has predicted the proton affinity of HCS^+ very accurately, it can be inferred that it will also predict the proton affinity of HSC^+ accurately as well.

Table 3a. Proton Affinity values of CS

Method	Proton attached to C atom		Proton attached to S atom	
	PA (kcal/mol)	Error	PA (kcal/mol)	Error
Experimental	189.200	NA	-	-
G4	190.409	1.209	119.191	-
MP2/6-311$^+$	193.599	4.399	113.732	-
MP2/cc-pVDZ	191.095	1.895	112.771	-
CCSD/ cc-pVDZ	189.360	0.060	121.204	-
W2U	189.280	0.080	117.560	-

3.3.2 Bond Lengths and Bond angle of HCS^+

In HCS^+, hydrogen is added to the carbon atom, forming an asymmetric structure. The hydrogen atom introduces additional electron density to the carbon-sulfur bond region. This increased electron density leads to greater repulsion between the electrons in the bond, causing the carbon-sulfur bond to stretch, leading to an increase in bond length.

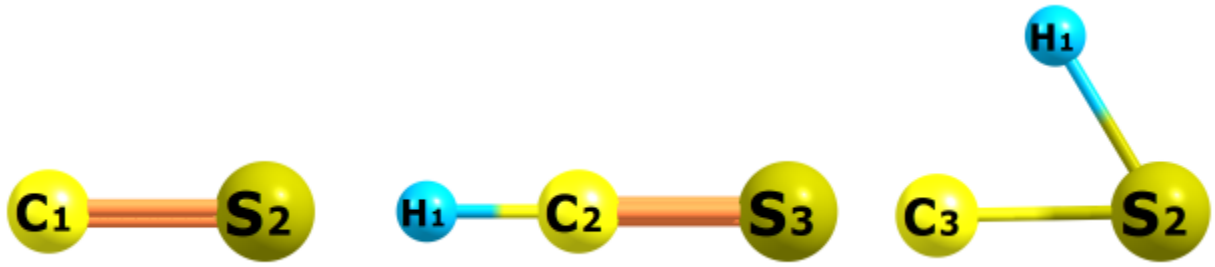

Fig. 3a. Optimized geometries of CS, HCS^+ and HSC^+

In HSC^+, hydrogen is added to the sulfur atom, also resulting in an asymmetric structure. The presence of hydrogen near sulfur affects the electron distribution in the carbon-sulfur bond. The hydrogen atom is electron-donating, which can result in an increased electron density around sulfur. This increased electron density strengthens the carbon-sulfur bond, causing it to contract, resulting in a shorter bond length. When hydrogen is added to either carbon or sulfur in carbon monosulfide, the bond length between carbon and sulfur changes due to alterations in the molecular structure and electron distribution. Adding hydrogen to carbon results in an elongation of the bond, while adding hydrogen to sulfur leads to a contraction of the bond length. These changes in bond length reflect the redistribution of electron density and the resulting alterations in the bonding interactions within the molecule.

Table 3b. Bond Lengths and Bond Angles of CS, HSC^+ and HCS^+

Bond lengths, R (Å) and Bond angles, A (º) of CS, CHS^+ and HCS^+							
		Expt	**G4**	**CCSD/ CC-PVDZ**	**W2U**	**MP2/6-311***	**MP2/CC-PVDZ**
	R(H1-S2)	-	1.371	1.374	1.397	1.391	1. 474
HSC^+	**R(S2-C3)**	-	1.642	1.649	1.611	1.682	1.611
	A(H1-S2-C3)	-	99.4º	99.2º	76.4º	93.5º	60º
HCS^+	**R(H1-C2)**	-	1.084	1.097	1.081	1.091	1.096
	R(C2-S3)	-	1.476	1.497	1.471	1.482	1.508
	A(H1-C2-S3)	-	180º	180º	180º	180º	180º
CS	**R(C1-S2)**	1.547	1.557	1.555	1.532	1.559	1.531

3.3.3 Rotational Constants

The rotational constants of HCS^+ are approximately 0.00 GHz, 21.34 GHz, and 21.34 GHz. HCS^+ has a linear geometry with hydrogen added to the carbon atom. As a linear molecule, it possesses two rotational degrees of freedom, leading to two identical rotational constants (B and C) representing rotations about two perpendicular axes, perpendicular to the molecule's axis.

While the rotational constants of HSC^+ are approximately 337.4 GHz, 19.38 GHz, and 18.327 GHz. HSC^+ has a linear geometry with hydrogen added to the sulfur atom. Like HCS^+, it also has two rotational degrees of freedom, resulting in two identical rotational constants (B and C). The rotational constants of carbon monosulfide are 0.00 GHz, 20.04 GHz, and 20.04 GHz. CS is linear and does not need hydrogen addition. It has just one rotational degree of freedom as a linear molecule, resulting in two equal rotational constants (B and C).

HCS^+, HSC^+, and CS have rotational constants that reflect the varied molecular geometries and moments of inertia of these compounds. Because of their linear structures with hydrogen addition, HCS^+ and HSC^+ have comparable rotational constants, but CS, being a linear molecule, has somewhat different rotational constants.

Table 3d. Rotational Constants of HSC^+, HCS^+ and CS

Method		Rotational Constants (Ghz)		
		A	**B**	**C**
	Experimental	0.000	24.5844	24.5844
	G4	0.000	20.0422	20.0422
CS	**MP2/cc-pvdz**	0.000	20.0422	20.0422
	CCSD/ cc-pvdz	0.000	23.9423	23.9423
	W2U	0.000	20.0422	20.0422
	MP2/6-311*	0.000	21.0346	21.0346
	Experimental	-	-	-
	G4	0.000	21.414	21.414
HCS^+	**MP2/cc-pvdz**	0.000	21.414	21.414
	CCSD/ cc-pvdz	0.000	21.414	21.414
	W2U	0.000	21.571	21.571
	MP2/6-311*	0.000	21.462	21.462
	Experimental	-	-	-
	G4	337.4	19.38	18.327
HSC^+	**MP2/cc-pvdz**	337.4	19.38	18.327
	CCSD/ cc-pvdz	337.4	19.38	18.327
	W2U	337.4	19.38	18.327
	MP2/6-311*	337.4	19.38	18.327

3.3.4 Dipole Moment

The polarity of molecules' bonds and molecular geometry impact their dipole moments. Carbon monosulfide (CS) has a linear structure with a polar C=S bond, resulting in an unequal distribution of electron density due to the electronegativity difference between carbon and sulfur. However, because of the symmetry of the linear structure, the dipole moments are partially cancelled, resulting in a significantly lower total dipole moment of 0.5804 Debye. In the case of HCS^+, however, the addition of hydrogen to the carbon atom disrupts molecular symmetry and strengthens the polar C=S bond, resulting in a higher dipole moment of 2.0655 Debye.

Similarly, in HSC^+, the addition of hydrogen to sulfur also disrupts the molecular symmetry, contributing to a substantial dipole moment of 1.625 Debye. Thus, the differing dipole moments in these molecules are due to variations in bond polarity and molecular

geometry arising from the addition of hydrogen atoms to different atoms within the carbon monosulfide molecule.

3.3.5 Vibrational Frequencies

The observed vibrational frequencies and peaks in HCS^+ (hydrogen added to carbon in carbon monosulfide) and HSC^+ (hydrogen added to sulfur in carbon monosulfide) are due to the molecular structures and bonding characteristics introduced by the presence of hydrogen atoms. HCS^+ and HSC^+ both have linear geometries, and the addition of hydrogen atoms to either carbon or sulfur does not significantly alter their fundamental vibrational modes compared to the parent molecule, CS.

Table 3f. Dipole Moments of HCS^+, HSC^+ and CS

Method	Dipole Moment (Debye) HCS	Dipole moment (Debye) CSH	Dipole moment (Debye) CS
Experimental	-	-	1.958
G4	2.0655	1.6247	1.6028
MP2/cc-pvdz	2.0655	1.6247	0.5804
CCSD/ cc-pvdz	2.0655	1.5598	1.3503
W2U	1.6325	1.4710	1.2519
MP2/6-311*	2.0563	1.5836	1.0213

This similarity in molecular structure results in four very similar vibrational frequencies corresponding to symmetric and asymmetric stretching modes, and bending modes, leading to three very similar peaks in their infrared spectra. In contrast, CS has a linear molecular structure without the added complexity of hydrogen atoms, resulting in only one vibrational frequency corresponding to symmetric and asymmetric stretching of the C=S bond. The presence of hydrogen alters the frequencies by influencing the molecular geometry and bonding interactions. The added hydrogen atoms introduce additional vibrational degrees of freedom and changes in bond strengths, leading to variations in vibrational frequencies and observed peaks in the infrared spectra of HCS^+ and CHS^+ compared to the simpler vibrational spectrum of CS.

Table 3g. Vibrational Frequencies of HSC^+, HCS^+ and CS

	Vibrational Frequencies (cm^{-1})					
	Experimental	**G4**	**CCSD/ CC-PVDZ**	**W2U**	**MP2/6-311***	**MP2/CC-PVDZ**
	-	835.7864	765.9	807.5047	785.2125	765.9
	-	835.7864	765.9	807.5047	285.2125	765.9
HCS^+	-	1453.6385	1442.3	1461.2534	1451.6154	1386.4
	-	3298.9679	3289.1	3269.5094	3255.2384	3298.7
CS	1272.000	1295.6909	1317.7016	1312.598	1351.7690	1295.5931
	-	835.7864	765.9	807.5047	785.2125	785.9
HSC^+	-	835.7864	765.9	807.5047	285.2125	785.9
	-	1453.6385	1442.3	1461.2534	1451.6154	1734.4
	-	3298.9679	3289.1	3269.5094	3255.2384	3205.7

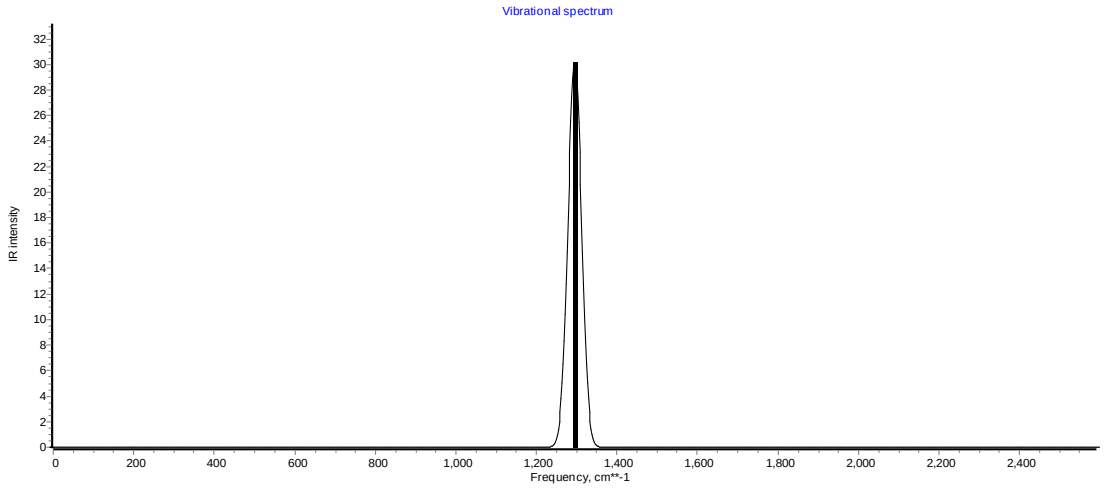

Fig. 3b. Calculated IR Intensities for CS

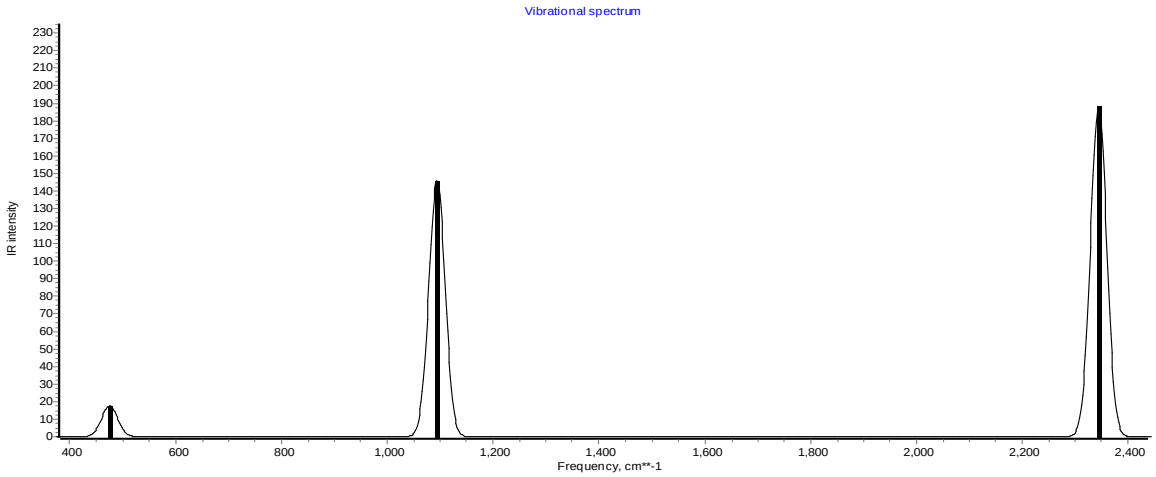

Fig. 3c. Calculated IR Intensities for HSC^+

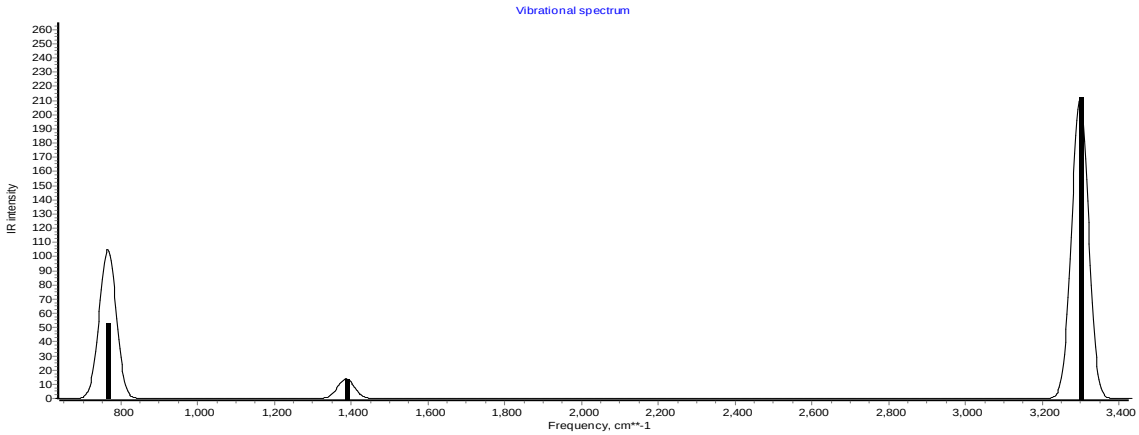

Fig. 3d. Calculated IR Intensities for HCS

3.4. Hydrogen H_2

3.4.1 Proton Affinity

The proton affinity of hydrogen is an important concept in chemistry, as it quantifies the willingness of a hydrogen atom to accept an additional proton. Since hydrogen has only one electron in its valence shell, it readily accepts a proton to achieve a stable electron configuration similar to helium (He), which has a full valence shell. The proton affinity of hydrogen is an essential factor in various chemical reactions, particularly in the study of ionization processes and the behavior of hydrogen ions in different environments. The proton affinity of hydrogen is approximately 101 kcal/mol, representing the energy change associated with the addition of a proton to a hydrogen atom and providing valuable insights into hydrogen's reactivity and interactions in various chemical systems. The results clearly show that the CCSD/CC-pvdz method is the most efficient in predicting the proton affinity of molecules.

Table 4a. Proton Affinity values of H_2

Method	Proton Affinity (KCal/mol)
Experimental	101.00
G4	96.75
MP2/cc-pvdz	96.19
CCSD/ cc-pvdz	98.76
W2U	94.08
MP2/6-311*	94.01

3.4.1 Bond lengths and bond angles of H_3^+

The molecular structure and bonding arrangements can explain the difference in bond lengths between H_2 and hydrogen-to-hydrogen in H_3^+ (hypothetical hydrogen trimer). The two hydrogen atoms in H_2 form a stable, diatomic molecule with a covalent link, with each hydrogen atom sharing a single pair of electrons, resulting in a bond length of around 0.74 angstroms (Å). Because of the dense electron cloud between the hydrogen nuclei, the connection is relatively strong. The bonding situation in H_3^+ is more complicated, assuming a triangle molecule shape in which each hydrogen atom is connected to the other two. This arrangement introduces additional electron-electron repulsions, slightly weakening the bonds, leading to a longer hydrogen-to-hydrogen bond length of approximately 0.9 angstroms (Å) in the hypothetical H_3^+ structure. It's important to note that H_3^+ is a theoretical concept and not a stable molecule under normal conditions, and the bond lengths discussed are approximate values used in theoretical investigations and models.

The bond angle of the hypothetical hydrogen trimer (H_3^+) is 60 degrees due to its triangular molecular geometry. In the H_3^+ structure, three hydrogen atoms are arranged in an equilateral triangle, forming covalent bonds between each other. In such a symmetric configuration, the angles between the hydrogen-hydrogen bonds are identical, resulting in bond angles of 60 degrees. The equilateral triangle is the most stable arrangement for H_3, as it maximizes the spacing between the hydrogen nuclei while minimizing electron-electron repulsions. This molecular geometry with bond angles of 60 degrees is characteristic of a symmetric, planar structure, and it reflects the symmetry and stability of the hypothetical hydrogen trimer. However, it's important to note that H_3^+ is a theoretical concept and does not exist as a stable molecule under normal conditions.

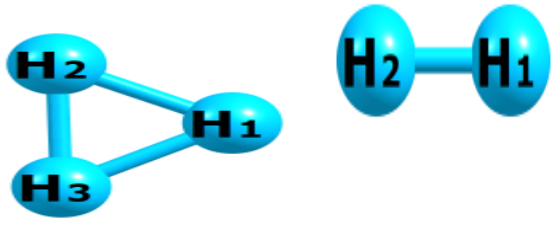

Fig.4a. Optimized Geometries of H_2 and H_3^+

Table 4b. Bond length and Bond angle values of H_3^+

Method	Bond Lengths (Å) H_3^+			Bond Angles (°)			Bond length H_2
	H1-H2	H2-H3	H1-H3	H1-H2-H3	H2-H3-H1	H3-H1-H2	H1-H2
Experimental	0.900	0.900	0.900	60°	60°	60°	0.740
G4	0.874	0.874	0.874	60°	60°	60°	0.743
MP2/cc-pvdz	0.896	0.896	0.896	60°	60°	60°	0.754
CCSD/ cc-pvdz	0.901	0.901	0.901	60°	60°	60°	0.740
W2U	0.880	0.880	0.880	60°	60°	60°	0.742
MP2/6-311*	0.851	0.851	0.851	60°	60°	60°	0.747

3.4.3 Rotational Constants

The difference in electronegativity between the atoms and the molecular geometry impacts the dipole moment of a molecule. In the instance of H_2, it is a linear molecule composed of two hydrogen atoms held together by a covalent connection. Hydrogen has the same electronegativity as oxygen, resulting in a nonpolar covalent bond, and so H_2 has a dipole moment of 0.00, 1831.465 and 1831.465 Debye. The molecular geometry changes to triangular with an equilateral triangle arrangement when hydrogen is added to H_2 to generate H_3^+ (hydrogen trimer). Because of the equal bond lengths and bond angles, this symmetry causes the partial cancellation of dipole moments. As a result, H_3^+ has dipole moments 1316.894, 1312.126 and 657.253 Debye.

The addition of hydrogen changes the molecular geometry from linear to triangular, resulting in the observable shift in the dipole moment of H_2 as it becomes H_3^+. The rotational constants of H_2 and H_3^+ are unrelated to their dipole moments because the rotational constants are determined by the molecular masses and geometry, but the dipole moment is determined by the molecule's electronegativity and symmetry.

Table 4c. Rotational constant values of H_3^+ and H_2

Method		Rotational Constants (Ghz)		
		A	B	C
	Experimental	0.000	1824.327	1824.327
	G4	0.000	1831.465	1831.465
H_2	**MP2/cc-pvdz**	0.000	1831.465	1831.465
	CCSD/ cc-pvdz	0.000	1831.465	1831.465
	W2U	0.000	1831.465	1831.465
	MP2/6-311*	0.000	1831.465	1831.465
	Experimental	-	-	-
	G4	1316.894	1312.126	657.253
H_3^+	**MP2/cc-pvdz**	1316.894	1312.126	657.253
	CCSD/ cc-pvdz	1236.244	1236.244	618.139
	W2U	1316.894	1312.126	657.253
	MP2/6-311*	337.4	19.38	18.327

3.4.4 Dipole Moment of H_3^+

The dipole moment of a molecule depends on the electronegativity difference between the atoms and the molecular geometry. In the case of H_2 (hydrogen gas), it is a homonuclear diatomic molecule, consisting of two hydrogen atoms bonded together. Hydrogen is a diatomic element with identical electronegativity, resulting in a purely covalent bond with equal electron sharing. As a result, there is no permanent charge separation along the molecular axis, leading to a dipole moment of 0.00 Debye in H_2.

H_3^+ (hydrogen trimer) is a hypothetical molecule consisting of three hydrogen atoms arranged in a triangular structure. Although hydrogen atoms have similar electronegativities, the triangular geometry introduces slight asymmetry, leading to a small charge separation along the molecular axis. This asymmetric distribution of electron density results in a permanent dipole moment for H_3, which is approximately 0.018 Debye.

Table 4d. Dipole moment values of H_3^+

Method	Dipole Moment (Debye) H_3^+	Dipole Moment (Debye) H_2
Experimental	-	0.000
G4	0.0018	0.000
MP2/cc-pvdz	0.0018	0.000
CCSD/ cc-pvdz	0.0000	0.000
W2U	0.0016	0.000
MP2/6-311*	0.0016	0.000

3.4.5 Vibrational frequencies

The difference in the number of vibrational frequencies and peaks between H_2 (hydrogen gas) and H_3^+ (hydrogen trimer) can be attributed to their molecular structures and bonding arrangements. H_2 is a homonuclear diatomic molecule with two hydrogen atoms bonded by a covalent bond. As a diatomic molecule, H_2 possesses only one vibrational degree of freedom, which corresponds to the stretching of the H-H bond. This single vibrational frequency results in one vibrational mode but does not give rise to any distinct peaks in the infrared spectrum, as the vibrational transition does not involve a change in the molecule's dipole moment.

On the other hand, H_3^+ consists of three hydrogen atoms arranged in a triangular structure. In this case, the asymmetric geometry introduces three vibrational degrees of freedom: two stretching modes (H-H bond stretching and symmetric bending) and one bending mode (out-of-plane bending). These three vibrational frequencies result in two distinct peaks in the infrared spectrum, as the vibrational transitions involve changes in the molecule's dipole moment. The increased complexity of the triangular structure in H_3^+ compared to the linear structure of H_2 leads to the observation of multiple vibrational frequencies and peaks in its infrared spectrum.

Table 4c. Vibrational frequency values of H_3^+ and H_2

		Vibrational Frequencies (cm^{-1})				
	Experimental	**G4**	**CCSD/ CC-PVDZ**	**W2U**	**MP2/6-311***	**MP2/CC-PVDZ**
	-	2737.9379	2665.582	2713.235	785.2125	2712.138
H_3^+	-	2743.6711	2665.712	2715.999	285.2125	2712.297

	-	3492.2382	3545.593	3410.233	1451.6154	3590.570
H_2	4161.2	4466.4384	4382.8819	4434.4137	4491.5425	4501.2610

Fig. 4b. Calculated IR Intensities for H_2

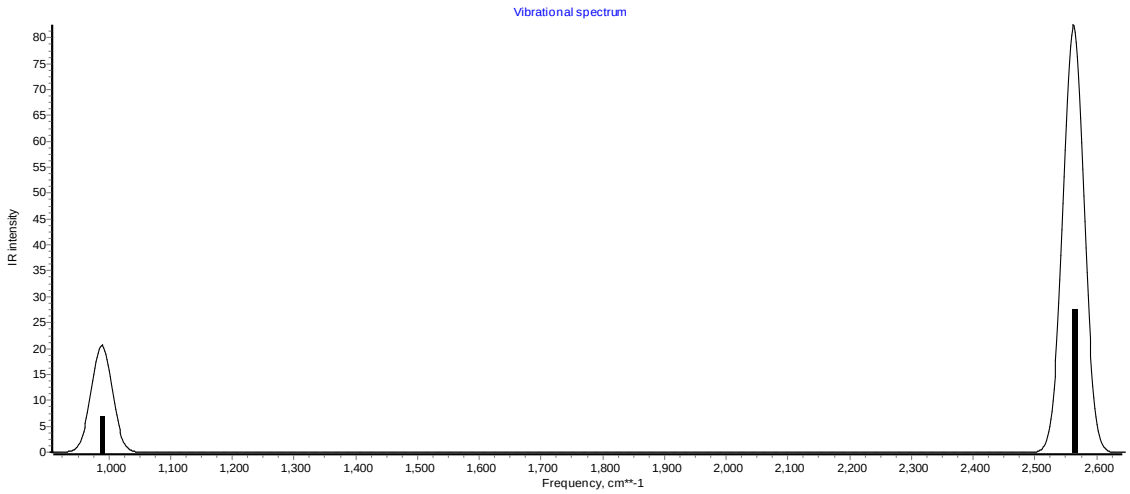

Fig. 4c. Calculated IR Intensities for H_3

3.5 Phosphine PH_3

3.5.1 Proton Affinity

The proton affinity of phosphine, which is approximately 188 kcal/mol, represents the energy required to add a proton (H^+) to a phosphine molecule (PH_3), converting it into a positively charged phosphonium ion (PH_4^+). This protonation process involves the transfer of a proton to the phosphorus atom in phosphine, resulting in the formation of the PH_4^+ cation. The relatively high proton affinity of phosphine indicates its favourable tendency to accept a proton and form the phosphonium ion. Understanding the proton affinity of phosphine is essential for studying its behavior in acidic environments and its involvement in

proton-transfer reactions, providing valuable insights into its chemistry and applications.

Table 5a. Proton Affinity values of PH_3

Method	Proton Affinity (kCal/mol)
Experimental	188.00
G4	186.58
MP2/cc-pvdz	186.99
CCSD/ cc-pvdz	187.36
W2U	186.17
MP2/6-311*	190.47

3.5.2 Bond lengths and Bond angles of PH_4^+

The bond lengths of phosphine (PH_3) are the same, while those of PH_4^+ (tetrahydridophosphonium ion) are different due to their respective molecular geometries. PH_3 has a trigonal pyramidal structure, with three hydrogen atoms bonded to a central phosphorus atom. The three P-H bonds are symmetrically arranged around the phosphorus atom, resulting in identical bond lengths. On the other hand, PH_4^+ has a tetrahedral molecular structure, with four hydrogen atoms surrounding the central phosphorus atom. In this arrangement, each hydrogen atom experiences different electron-electron repulsions based on their relative positions, leading to variations in bond lengths between the phosphorus atom and the individual hydrogen atoms. Consequently, the molecular geometry determines the uniformity or variation in bond lengths in phosphine and tetrahydridophosphonium ion.

Owing to the geometry of the molecule the corresponding tetrahedral molecular structure is the reason why PH_4^+ has a bond angle of 109.5 °.

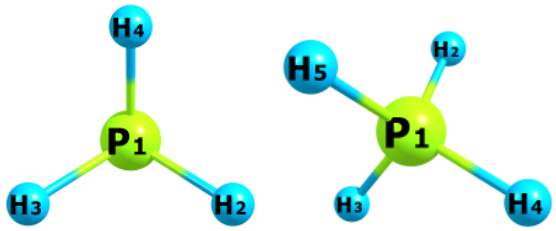

Fig.5a. Optimized geometries of PH_3 and PH_4^+

Table 5b. Bond Lengths of PH_4^+

Method	Bond Lengths (Å)PH_4^+				Bond Lengths (Å) PH_3		
	P1-H2	**P1-H3**	**P1-H4**	**P1-H5**	**P1-H2**	**P1-H3**	**P1-H4**
Experimental	-	-	-	-	1.422	1.422	1.422
G4	1.440	1.440	1.440	1.440	1.4142	1.4142	1.4142
MP2/cc-pvdz	1.402	1.402	1.402	1.402	1.412	1.412	1.412
CCSD/ cc-pvdz	1.406	1.406	1.406	1.406	1.4292	1.4294	1.4293
W2U	1.397	1.397	1.397	1.397	1.417	1.417	1.417
MP2/6-311*	1.414	1.414	1.414	1.414	1.440	1.440	1.440

3.5.3 Rotational Constants of PH_4^+

The rotational constants of PH_3 (phosphine) and PH_4^+ (tetrahydridophosphonium ion) differ due to their different molecular geometries and mass distributions. Three hydrogen atoms are linked to a central phosphorus atom in the trigonal pyramidal structure of PH_3.Because of the asymmetry of the molecular structure, moments of inertia vary at different axes, resulting in rotational constants of 147.7 GHz,

147.7 GHz, and 90.7 GHz. PH_4^+ has a tetrahedral molecular structure with four hydrogen atoms encircling the core posphorus atom, resulting in a more symmetric mass distribution.

The tetrahedral geometry's symmetry results in identical moments of inertia about all three major axes, resulting in rotational constants of 90.7 GHz, 90.7 GHz, and 90.7 GHz.

Overall, the differences in the rotational constants between PH_3 and PH_4^+ are directly related to their molecular geometries. The trigonal pyramidal structure of PH_3 results in non-equal rotational constants, while the tetrahedral structure of PH_4^+ yields identical rotational constants due to its symmetric mass distribution. Rotational spectroscopy provides valuable insights into the molecular structures and properties of molecules, helping to understand their rotational motion and behavior in the gas phase.

Table 5c. Bond Angles of PH_4^+

Method	Bond Angles (^{O}) PH_3^+						Bond Angles (^{O}) PH_3		
	2-1-3	**2-1-4**	**2-1-5**	**3-1-4**	**3-1-5**	**4-1-5**	**2-1-3**	**2-1-4**	**3-1-4**
Experimental	-	-	-	-	-	-			
G4	109.46	109.47	109.48	109.46	109.48	109.47	93.2	93.2	93.2
MP2/cc-pvdz	109.5	109.5	109.5	109.5	109.5	109.5	93.7	93.7	93.7
CCSD/ cc-pvdz	109.5	109.5	109.5	109.5	109.5	109.5	93.5	93.5	93.5
W2U	109.5	109.5	109.5	109.5	109.5	109.5	93.5	93.5	93.5
MP2/6-311*	109.46	109.46	109.47	109.47	147.73	147.71	93.4	93.4	93.4

Table 5d. Rotational Constant values of PH_3 and PH_4^+

Method		Rotational Constants (Ghz)		
		A	**B**	**C**
	Experimental	133.47839	133.47839	117.81844
	G4	132.9860	132.9860	117.4430
PH_3	**MP2/cc-pvdz**	134.1730	134.1730	117.581
	CCSD/ cc-pvdz	131.9408	131.935	115.575
	MP2/6-311*	147.7095	147.7095	90.6910
	W2U	135.4554	132.9983	117.453
	Experimental	-	-	-
	G4	90.694	90.684	90.679
PH_4^+	**MP2/cc-pvdz**	96.758	96.758	96.752
	CCSD/ cc-pvdz	95.683	95.680	95.678
	W2U	96.758	96.758	96.752
	MP2/6-311*	90.694	90.684	90.679

3.5.4 Dipole Moment of PH_4^+

The dipole moments of molecules are influenced by their molecular geometries and the distribution of charge within the molecule. In the case of PH_3 (phosphine), its dipole moment is 0.9287 Debye, indicating a polar molecule. The molecular structure of PH_3 is trigonal pyramidal, with three hydrogen atoms surrounding a central phosphorus atom. The asymmetric arrangement of atoms in the trigonal pyramidal structure results in an

uneven distribution of electron density, with a partial negative charge on the phosphorus atom and partial positive charges on the hydrogen atoms. This charge separation creates a net dipole moment along the P-H bonds, leading to the overall dipole moment observed in PH_3.

In contrast, PH_4^+ (tetrahydridophosphonium ion) has a dipole moment of 0.0002 Debye, indicating a nearly nonpolar molecule. The molecular geometry of PH_4^+ is tetrahedral, with four hydrogen atoms surrounding a central phosphorus atom. In this symmetrical arrangement, the charge distribution among the atoms is more uniform, resulting in a minimal net dipole moment. The partial positive charges on the hydrogen atoms are balanced by the partial negative charge on the phosphorus atom, leading to nearly cancelling dipole moments along the P-H bonds and an overall very small dipole moment for PH_4^+.

3.5.5 Vibrational Frequencies

PH_3, with its trigonal pyramidal structure, has six vibrational degrees of freedom due to its asymmetric geometry, leading to six distinct vibrational frequencies. Four of these vibrational frequencies result in sharp peaks in the infrared spectrum due to their strong and specific vibrational transitions.

Table 5e. Dipole Moment values of PH_4^+

Method	Dipole Moment (Debye) PH_4^+	Dipole Moment (Debye) PH_3
Experimental	-	0.580
G4	0.0001	0.6654
MP2/cc-pvdz	0.0001	0.7345
CCSD/ cc-pvdz	0.0002	0.6835
W2U	0.0000	0.5907
MP2/6-311*	0.0002	0.7252

On the other hand, PH_4^+'s tetrahedral structure introduces eight vibrational degrees of freedom, resulting in eight vibrational frequencies. However, only two of these vibrational frequencies lead to sharp peaks in the infrared spectrum, while the others may be either weak or not distinguishable due to symmetry considerations. Thus, the molecular geometries and vibrational modes of PH_3 and PH_4^+ , revealed by spectroscopic analysis, account for the differences in the number of vibrational frequencies and sharp peaks observed in their respective infrared spectra.

Table 5f. Vibrational Frequency values of PH_3 and PH_4^+

Vibrational Frequencies (cm^{-1})						
	Experimental	**G4**	**CCSD/ CC-PVDZ**	**W2U**	**MP2/6-311***	**MP2/CC-PVDZ**
	-	988.6942	996.6370	992.3401	1043.8424	1010.1952
	-	988.8004	996.6395	992.7515	1043.8445	1010.1961
	-	1133.974	996.6452	992.7894	1043.8481	1010.1979
PH_4^+	-	1134.050	1136.0963	1135.8659	1177.3561	1158.5224
	-	2508.586	1136.1022	1135.8659	1177.3615	1158.5241
	-	2508.586	2547.8803	1136.1964	2616.4124	2589.2426
	-	2562.539	2602.7259	2503.1235	2666.9365	2650.6764

	-	2562.706	2602.7316	2554.1243	2666.9380	2650.6769
	992.0	1025.0859	1041.4147	1021.3525	1050.1976	1038.8461
PH_3	1118.0	1142.7923	1151.5288	1140.7894	1156.5851	1162.8901
	1118.0	1142.7923	1151.5353	1141.1317	1156.6207	1162.8901
	2323.0	2388.9482	2427.5212	2390.8596	2510.5756	2487.2606
	2328.0	2398.8036	2427.5212	2397.2363	2519.1242	2504.8423
	2328.0	2398.8038	2437.9721	2397.9504	2520.0142	2504.8520

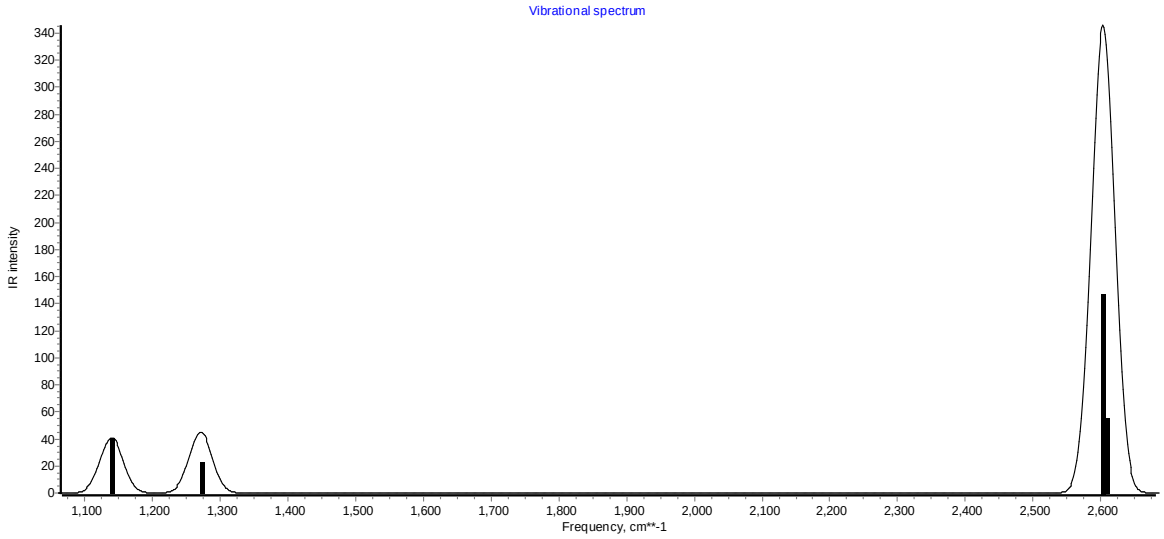

Fig 5b. Calculated IR Intensities for PH_3

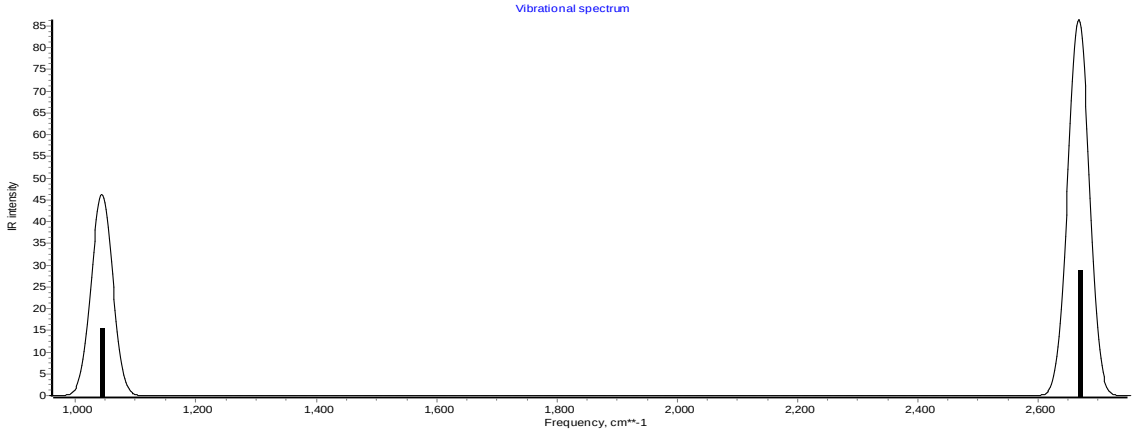

Fig. 5c. Calculated IR Intensities for PH_4^+

4.0 Conclusion

In conclusion, this research investigated the influence of protonation on the structural and spectroscopic properties of molecules, focusing on N_2, CO, H_2, CS, and PH_3. Through computational studies using various methods

such as G4, MP2/6-311*, MP2/CC-pvdz, CCSD/CC-pvdz, and W2U, valuable insights were gained into the protonation processes and their effects on the molecules' behaviors. The results revealed that protonation significantly affects the molecular geometries, vibrational frequencies, dipole moments, and proton affinity values of the studied molecules. The protonation of these molecules led to the formation of charged species, revealing the potential for their involvement in various chemical reactions and the ability to act as reactive intermediates in different environments. The computational methods employed in this research proved to be powerful tools for understanding the intricate structural and spectroscopic changes induced by protonation. The Coupled cluster method provided very accurate results in regards to the experimental data available. The findings of this study enhance our fundamental understanding of protonation reactions and their implications in molecular reactivity, providing valuable knowledge for future studies in chemistry and related fields.

5.0 References

Agúndez, M., Cernicharo, J., De Vicente, P., Marcelino, N., Roueff, E., Fuente, A., ... & Tercero, F. (2015). Probing non-polar interstellar molecules through their protonated form: Detection of protonated cyanogen ($NCCNH^+$). *Astronomy & Astrophysics*, *579*, L10.

Baiz, C. R., Błasiak, B., Bredenbeck, J., Cho, M., Choi, J. H., Corcelli, S. A., ... & Zanni, M. T. (2020). Vibrational spectroscopic map, vibrational spectroscopy, and intermolecular interaction. *Chemical reviews*, *120, 15, pp.* 7152-7218.18.

Benkyi, I., Tapavicza, E., Fliegl, H., & Sundholm, D. (2019). Calculation of vibrationally resolved absorption spectra of acenes and pyrene. *Physical Chemistry Chemical Physics*, *21, 37, pp.* 21094-21103.

Ben-Shimon, A., Shalev, D. E., & Niv, M. Y. (2013). Protonation States in molecular dynamics simulations of peptide folding and binding. *Current pharmaceutical design*, *19, 23, pp.* 4173-4181.

Bodenstein, T., & Kvaal, S. (2020). A state-specific multireference coupled-cluster method based on the bivariational principle. *The Journal of Chemical Physics*, *153*(2).

Cabezas, C., Agúndez, M., Marcelino, N., Tercero, B., Fuentetaja, R., de Vicente, P., & Cernicharo, J. (2022). Discovery of a new molecular ion, $HC7NH^+$, in TMC-1. *Astronomy & Astrophysics*, *659*, L8.

Caselli, P., Sipilä, O., & Harju, J. (2019). Deuterated forms of $H3^+$ and their importance in astrochemistry. *Philosophical Transactions of the Royal Society A*, *377*(2154), 20180401.

Chen, B. W., Xu, L., & Mavrikakis, M. (2020). Computational methods in heterogeneous catalysis. *Chemical Reviews*, *121*(2), 1007-1048. Baiz, C. R., Błasiak, B., Bredenbeck, J., Cho, M., Choi, J. H., Corcelli, S. A., ... & Zanni, M. T. (2020).

Chen, J., Zhang, S., Wang, W., Sun, H., Zhang, Q., & Liu, X. (2021). Binding of inhibitors to BACE1 affected by pH-dependent protonation: An exploration from multiple replica Gaussian accelerated molecular dynamics and MM-GBSA calculations. *ACS Chemical Neuroscience*, *12*(14), 2591-2607.

Chester, S. M. (2019). Weizmann lectures on the numerical conformal bootstrap. *arXiv preprint arXiv:1907.05147*.

Cramer, C. J. (2013). *Essentials of computational chemistry: theories and models*. John Wiley & Sons.

DeFrees, D. J., & McLean, A. D. (1986). Ab initio determination of the proton affinities of small neutral and anionic molecules. *Journal of computational chemistry*, *7*(3), 321-333.

Eddy, N. O. & Ita, B. I. (2011). Experimental and theoretical studies on the inhibition potentials of some derivatives of cyclopenta-1,3-diene. *International Journal of Quantum Chemistry* 111, 14, pp. 3456-3473. DOI:10.1002/qua

Eddy, N. O. & Ita, B. I. (2011). Theoretical and experimental studies on the inhibition potentials of aromatic oxaldehydes for the corrosion of mild steel in 0.1 M HCl. *Journal of Molecular Modeling* 17, pp. 633-647. DOI:10.1007/s00894-010-0749

Etim, E. E., & Arunan, E. (2016). Interstellar isomeric species: Energy, stability and abundance relationship. *The European Physical Journal Plus*, *131*, pp. 1-10.

Etim, E. E., Gorai, P., Das, A., & Arunan, E. (2017). Interstellar protonated molecular species. *Advances in Space Research*, *60*(3), 709-721.

Etim, E. E., & Oko Emmanuel, G. (2020). Protonation in Heteronuclear Diatomic Molecules: Same Molecule, Different Proton Affinities. *Communication in Physical Sciences*, *6*(2) 835-844.

Gaussian09, R. A. (2009). 1, mj frisch, gw trucks, hb schlegel, ge scuseria, ma robb, jr cheeseman, g. Scalmani, v. Barone, b. Mennucci, ga petersson et al., gaussian. *Inc., Wallingford CT*, *121*, 150-166.

Herbst, E. (2017). The synthesis of large interstellar molecules. *International Reviews in Physical Chemistry*, 36, 2*, pp.* 287-331.

Keith, J. A., Vassilev-Galindo, V., Cheng, B., Chmiela, S., Gastegger, M., Müller, K. R., & Tkatchenko, A. (2021). Combining machine learning and computational chemistry for predictive insights into chemical systems. *Chemical reviews*, 121, 16, pp. 9816-9872.

Knauth, D. C., Andersson, B. G., McCandliss, S. R., & Warren Moos, H. (2004). The interstellar N2 abundance towards HD 124314 from far-ultraviolet observations. *Nature*, *429*(6992), 636-638.

Krynski, M., & Rossi, M. (2021). Efficient Gaussian process regression for prediction of molecular crystals harmonic free energies. *npj Computational Materials*, *7*(1), 169.

Larsson, M., McCall, B. J., & Orel, A. E. (2008). The dissociative recombination of $H3^+$ –a saga coming to an end?. *Chemical Physics Letters*, *462, 4-6, pp.* 145-151.

Mata, R. A. (2010). Application of high level wavefunction methods in quantum mechanics/molecular mechanics hybrid schemes. *Physical Chemistry Chemical Physics*, *12, 19, pp.* 5041-5052.

Montes de Oca-Estevez, M. J., & Prosmiti, R. (2021). Computational Characterization of Astrophysical Species: The Case of Noble Gas Hydride Cations. *Frontiers in Chemistry*, *9*pp, 664693.

Nair, A. S., & Pathak, B. (2021). Computational strategies to address the catalytic activity of nanoclusters. *Wiley Interdisciplinary Reviews: Computational Molecular Science*, *11, 4,* , e1508.

Nguyen, Q. T., Tran, P., Ngo, T. D., Tran, P. A., & Mendis, P. (2014). Experimental and computational investigations on fire resistance of GFRP composite for building façade. *Composites Part B: Engineering*, *62*, pp. 218-229.

Noble, J., Dedonder-Lardeux, C., & Jouvet, C. (2019). Excited States Processes in Protonated Molecules Studied by Frequency-Domain pectroscopy. *Physical Chemistry of Cold Gas-Phase Functional Molecules and Clusters*, 337-365.

Re, S., Watabe, S., Nishima, W., Muneyuki, E., Yamaguchi, Y., MacKerell Jr, A. D., & Sugita, Y. (2018). Characterization of conformational ensembles of protonated N-glycans in the gas-phase. *Scientific Reports*, *8*(1), 1644.

Thaddeus, P., Guélin, M., & Linke, R. A. (1981). Three

new'nonterrestrial'molecules. *The Astrophysical Journal*, *246*, pp. L41-L45.

Turner, A. M., Koutsogiannis, A. S., Kleimeier, N. F., Bergantini, A., Zhu, C., Fortenberry, R. C., & Kaiser, R.I. (2020). An experimental and theoretical investigation into the formation of ketene (H2CCO) and ethynol (HCCHO) in interstellar analog ices. *The Astrophysical Journal*, *896, 1, pp.* 88.

Wang, S., Kind, T., Tantillo, D. J., & Fiehn, O. (2020). Predicting in silico electron ionization mass spectra using quantum chemistry. *Journal of cheminformatics*, *12, 1, pp.* 1-11.

Declarations

The authors declare that they have no conflict of interest.

Data availability

All data used in this study will be readily available to the public.

Consent for publication

Not Applicable

Availability of data and materials

The publisher has the right to make the data Public.

Competing interests

The authors declared no conflict of interest.

Funding

There is no source of external funding

Authors' contributions

EEE conceived the idea. JPS carried out the computational calculations. AIO, EEE and JPS wrote the initial drafts. All authors revised the manuscript and made appropriate input.